



Article

Facile Synthesis of MoP-RuP₂ with Abundant Interfaces to Boost Hydrogen Evolution Reactions in Alkaline Media

Zhi Chen, Ying Zhao, Yuxiao Gao, Zexing Wu * and Lei Wang *

State Key Laboratory Base of Eco-Chemical Engineering, College of Chemistry and Molecular Engineering, Qingdao University of Science & Technology, 53 Zhengzhou Road, Qingdao 266042, China; 2020050008@mails.qust.edu.cn (Z.C.); zhaoying99up@163.com (Y.Z.); 2020050019@mails.qust.edu.cn (Y.G.)

* Correspondence: splswzx@qust.edu.cn (Z.W.); inorchemwl@126.com (L.W.)

Abstract: Exploiting efficient electrocatalysts for hydrogen evolution reactions (HERs) is important for boosting the large-scale applications of hydrogen energy. Herein, MoP-RuP₂ encapsulated in N,P-codoped carbon (MoP-RuP₂@NPC) with abundant interfaces were prepared via a facile avenue with the low-toxic melamine phosphate as the phosphorous resource. Moreover, the obtained electrocatalyst possessed a porous nanostructure, had abundant exposed active sites and improved the mass transport during the electrocatalytic process. Due to the above merits, the prepared MoP-RuP₂@NPC delivered a greater electrocatalytic performance for HERs (50 mV@10 mA cm⁻²) relative to RuP₂@NPC (120 mV) and MoP@NPC (195 mV) in 1 M KOH. Moreover, an ultralow potential of 1.6 V was required to deliver a current density of 10 mA cm⁻² in the two-electrode configuration for overall water splitting. For practical applications, intermittent solar energy, wind energy and thermal energy were utilized to drive the electrolyzer to generate hydrogen gas. This work provides a novel and facile strategy for designing highly efficient and stable nanomaterials toward hydrogen production.

Keywords: electrocatalyst; hydrogen evolution reaction; interfaces



Citation: Chen, Z.; Zhao, Y.; Gao, Y.; Wu, Z.; Wang, L. Facile Synthesis of MoP-RuP₂ with Abundant Interfaces to Boost Hydrogen Evolution Reactions in Alkaline Media. *Nanomaterials* **2021**, *11*, 2347. <https://doi.org/10.3390/nano11092347>

Academic Editor: Nikolaos Dimitratos

Received: 3 August 2021

Accepted: 4 September 2021

Published: 9 September 2021

Publisher's Note: MDPI stays neutral with regard to jurisdictional claims in published maps and institutional affiliations.



Copyright: © 2021 by the authors. Licensee MDPI, Basel, Switzerland. This article is an open access article distributed under the terms and conditions of the Creative Commons Attribution (CC BY) license (<https://creativecommons.org/licenses/by/4.0/>).

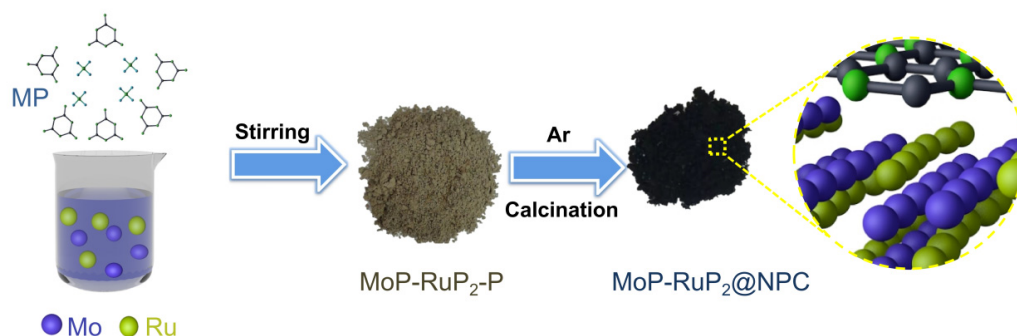
1. Introduction

Hydrogen is attracting significant attention around the world due to its high energy density, eco-friendly and sustainable merits, which favor alleviating the ever-increasing environmental pollution and energy crisis [1–7]. Among the developed technologies, electrochemical water splitting is regarded as an efficient and sustainable approach for hydrogen production [8–14]. As a half-reaction of water-splitting, the cathodic HER efficiency acts as a key role in reducing the energy consumption during hydrogen generation. Thus, it is of importance to develop electrocatalysts with advantageous catalytic performance for HERs [15–21]. At present, Pt-based nanomaterials are still the state-of-the-art electrocatalysts for HERs due to having the lowest overpotential and the smallest Tafel slope [22–24]. Unsatisfactorily, the scarcity and exorbitant price severely impede their widespread practical applications. Therefore, it is still worth developing alternatives to reduce the costs and accelerate the large-scale application of hydrogen energy in the actual environment [25,26].

Until now, a vast range of non-precious metal-based catalysts (e.g., metal sulfides [27–29], metal phosphides [30–32], metal carbides [33,34] and nonmetal-derived electrocatalysts [35,36]) have been investigated as substitutes for Pt for HERs [37,38]. However, compared with Pt-based electrocatalysts, the electrocatalytic activity of alternatives still lags [39]. More recently, tremendous efforts were made to explore other cost-effective precious metals (e.g., Pd, Ir and Ru) for promoting the HER catalytic activities due to their similar electron structures. Among them, ruthenium (Ru) is economically advantageous since the price is only one-fifteenth that of Pt. Moreover, the favorable Ru-H bond strength is also beneficial for boosting the reaction kinetics of HERs [40]. However, the electrocatalytic

performance of Ru-derived nanomaterials still needs to improve further. As reported, the created interfaces in the developed electrocatalysts can regulate the adsorption/desorption of intermediates, tune the transportation of electrons and expose more active sites during electrocatalytic processes [41–43]. For instance, Fu and co-authors [44] constructed 2D MoP/MoS₂ heterostructure nanosheets using two steps, namely, hydrothermal and phosphorization processes. The heterostructure catalyst helps to expose more active sites, thereby effectively activating H₂O and achieving good electron transfer. Because of the above advantage, the obtained MoP/MoS₂ presented an excellent electrocatalytic performance for HERs in neutral, alkaline and acid media. Structural and theoretical analysis results demonstrated that the surface of an MoP/MoS₂ heterostructure accelerates H⁺ and H₂O adsorption due to the stronger interaction between MoS₂ and MoP. Therefore, developing electrocatalysts with abundant interfaces is a promising avenue for boosting the electrocatalytic performance and lowering the content of noble metals.

Herein, we describe the fabrication of MoP-RuP₂@NPC with abundant interfaces via a facile one-step method, with the low-toxic melamine phosphate (MP) as the N and P resource (Scheme 1). The obtained electrocatalyst had rich interfaces and abundant pores, which allowed for the mass transport and acceleration of the reaction kinetics for HERs. Furthermore, the N,P-codoped carbon shell enhanced the electrochemical conductivity and protected against corrosion. Due to the above merits, the obtained MoP-RuP₂@NPC presented remarkable catalytic activity and stability for HERs. Interestingly, the two-electrode setup was easily powered by sustainable energies, including solar, wind and biomass energies.



Scheme 1. Schematic illustration of the synthesis of MoP-RuP₂@NPC.

2. Materials and Methods

2.1. Synthesis of MoP@NPC

Melamine phosphate (MP, 224 mg) and (NH₄)₆Mo₇O₂₄·4H₂O (58 mg) were uniformly dispersed in 20 mL of deionized water. The above solution was heated at 75 °C and stirred continuously until a viscous liquid was obtained. Then, the product was dried in a vacuum system for 12 h. Afterward, the as-prepared powder was annealed at different temperatures (700 °C, 800 °C and 900 °C) for 2 h under an Ar atmosphere with a flow rate of 2 °C min⁻¹. RuP₂@NCP was synthesized using the identical method with the addition of RuCl₃ (11.5 mg). MoP-RuP₂@NCP was synthesized in co-existence with RuCl₃ (11.5 mg) and (NH₄)₆Mo₇O₂₄·4H₂O (58 mg).

2.2. Physical Characterization

X-ray diffraction (XRD, X'Pert PRO) and X-ray photoelectron spectroscopy (XPS, AXIS SUPRA) were performed to identify the crystal structure and chemical composition. Scanning electron microscopy (SEM) and transmission electron microscopy (TEM) were conducted on a Regulus 8100 and a JEM-F200, respectively, to study the nanostructures of the prepared electrocatalysts.

2.3. Electrochemical Measurements

The electrocatalytic measurements were investigated using a three-electrode configuration with carbon rods, a reversible hydrogen electrode (RHE) and a glassy carbon electrode (5 mm in diameter), which were utilized as the counter electrodes, reference electrodes and working electrodes, respectively. A total of 5 mg of catalyst was dispersed in isopropanol solution (1 mL) with 20 μ L Nafion solution (Shanghai, China 5 wt%) and then sonicated for 50 min to form a homogeneous ink. Then, 20 μ L of the ink was dripped onto the glassy carbon electrode (containing 0.10 mg of catalyst). The electrocatalytic performance for HER was measured in a 1.0 M KOH medium. Linear sweep voltammograms (LSVs) were collected with a scanning rate of 5 mV s⁻¹. Long-term durability measurements were conducted with a specific potential. All electrochemical studies were investigated at room temperature.

3. Results and Discussion

X-ray diffraction (XRD) measurements were used to characterize the structure of the prepared electrocatalyst. We identified that the designed MoP-RuP₂@NPC was composed of MoP (PDF# 24-0771) and RuP₂ (PDF# 34-0333) (Figure 1a). As reference samples, RuP₂@NPC and MoP@NPC were composed of RuP₂ and MoP, respectively (Figure S1). The morphology and structure of the obtained electrocatalyst were studied using scanning electron microscopy (SEM) and transmission electron microscopy (TEM). The panoramic SEM image (Figure 1b) shows that abundant interconnected pores existed in the designed nano-materials, which could expose rich active sites and benefit the mass transport during the electrocatalytic process. The TEM images (Figure 1c) demonstrate that the developed MoP-RuP₂@NPC was composed of numerous connected nanoparticles. In the high-resolution TEM image (Figure 1d), the layer distances of 0.31 nm and 0.23 nm were ascribed to the (001) and (111) lattice planes of MoP and RuP₂, respectively, demonstrating the existence of MoP and RuP₂ in the obtained electrocatalyst. Interestingly, obvious interfaces were observed in the prepared MoP-RuP₂@NPC, which had a pivotal role in improving the electrocatalytic performance. The energy-dispersive X-ray spectrum (EDX) elemental mapping, shown in Figure 1e–k, revealed the homogenous distributions of Ru, Mo, C, O, P and N in the obtained MoP-RuP₂@NPC.

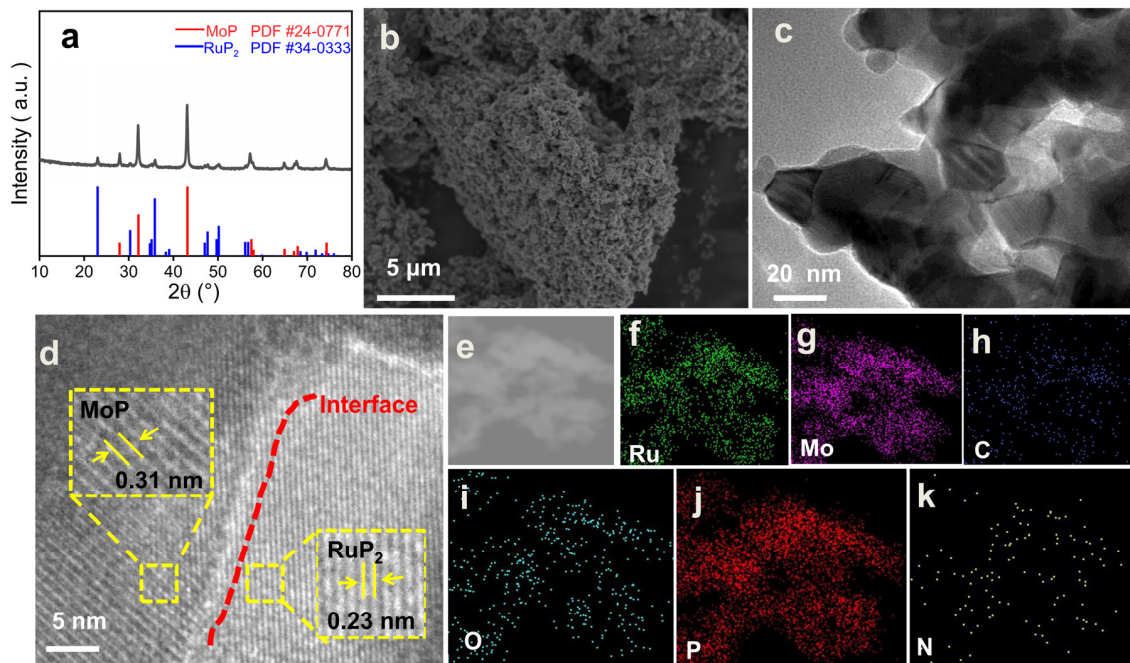


Figure 1. XRD (a), SEM (b) and TEM (c) images of MoP-RuP₂@NPC; (d) HRTEM image; (e) TEM/EDS image; (f–k) elemental mapping images for Ru, Mo, C, O, P and N.

X-ray photoelectron spectroscopy (XPS) analyses were undertaken to further analyze the valence states and chemical composition. In line with the elemental mappings, the XPS survey spectra showed the existence of Ru, Mo, N, P, C and O elements in the prepared MoP-RuP₂@NPC (Figure 2a). The high-resolution XPS spectrum of Ru showed peaks of Ru 2p_{3/2} and Ru 2p_{1/2} at 462 and 484.31 eV, respectively, are attributed to RuP₂ [45,46], as shown in Figure 2b. For the high-resolution spectra of Mo 3d (Figure 2c), the binding energies at 228.5 and 231.80 eV could be assigned to Mo^{δ+} species (0 < δ < 4), which are normally connected with the molybdenum species in MoP [47]. The other weak peaks at 229.2, 231.7 eV and 233.5, 236.0 eV could be attributed to MoO₂ and MoO₃ species, respectively, owing to oxidation in the air condition [48]. The doublet peaks at 129.8 and 130.6 eV in the P 2p region could be assigned to metal–P bonds (Figure 2d) [49]. The other peak at 134.1 eV was attributed to P–O owing to oxidation after being exposed to air [50]. For the high-resolution XPS spectrum of N 1s (Figure 2e), the 397.6, 399.5 and 402.14 eV peaks corresponded to pyridinic N, pyrrolic N and graphitic N, respectively [51]. The peaks centered at 533.1 eV and 531.6 eV were attributed to hydroxy oxygen, the physically adsorbed and chemisorbed water or other surface species in O 1s (Figure 2f) [52]. The atomic concentration of MoP-RuP₂@NPC that was found using XPS (at%) is shown in Figure S2.

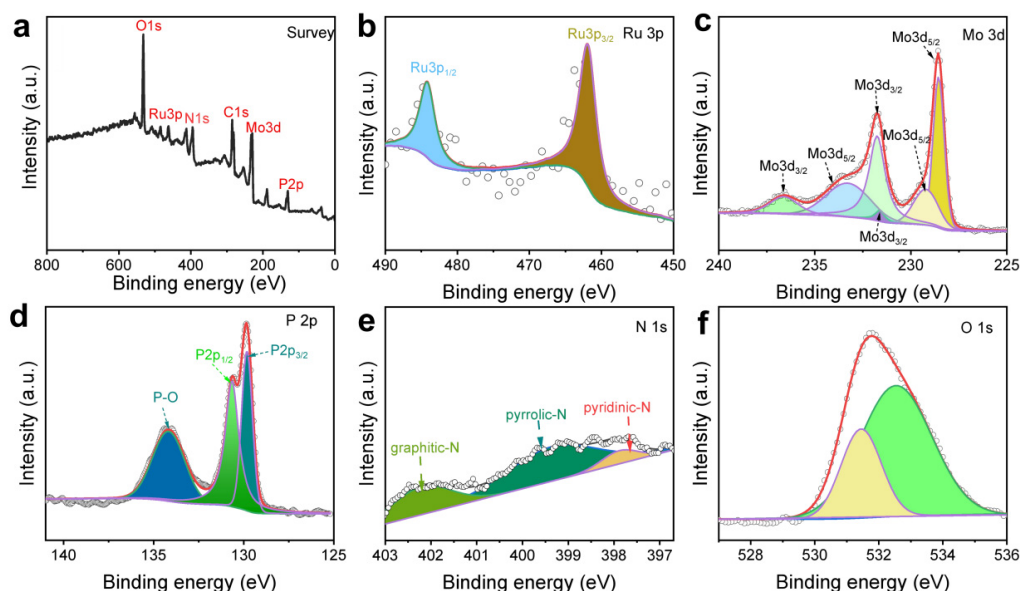


Figure 2. (a) The survey spectra for the MoP-RuP₂@NPC. High-resolution XPS spectra of Ru 3p (b), Mo 3d (c), P 2p (d), N 1s (e) and O 1s (f) of the MoP-RuP₂@NPC sample.

The electrocatalytic HER performance of the prepared catalyst was estimated in a 1.0 M KOH electrolyte on a standard three-electrode configuration. The contents of the Ru and pyrolysis temperatures were first investigated on regulating the catalytic activities for the HERs (Figures S3 and S4). The MoP-RuP₂@NPC with a molar ratio of 3:1 (Mo:Ru) at 800 °C presented the best catalytic performance for the HERs. As shown in Figure 3a, MoP-RuP₂@NPC possessed the smallest overpotential of 50 mV to achieve 10 mA cm⁻², relative to MoP@NPC (195 mV) and RuP₂@NPC (120 mV), demonstrating that the coexistence of RuP₂ and MoP was important for promoting the catalytic performances. The same tendency was also shown at a specific overpotential of 50 mV (Figure 3b). Moreover, the superior HER catalytic activity of MoP-RuP₂@NPC was further investigated using the Tafel curve (Figure 3c).

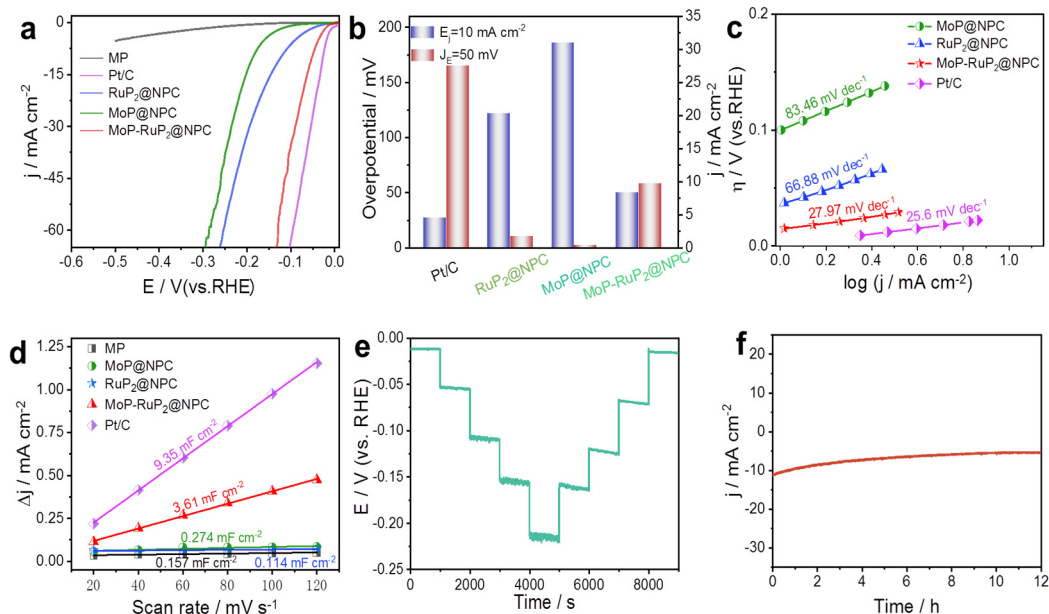


Figure 3. (a) LSVs of Pt/C, MoP-RuP₂@NPC, MoP@NPC, RuP₂@NPC and MP for the HERs with a scanning rate of 5 mV s⁻¹ in 1 M KOH. (b) Summarized overpotentials (current density of 10 mA cm⁻²) and the current density (overpotential of 50 mV vs. RHE). (c) Tafel slopes and (d) Cdl of the obtained nanomaterials. (e) Multistep chronoamperometric curves of MoP-RuP₂@NPC at various applied overpotentials in 1 M KOH. (f) Long-term stability study of the prepared electrocatalyst for 12 h.

The Tafel slope of MoP-RuP₂@NPC was only 27.97 mV dec⁻¹, much lower than MoP@NPC (83.46 mV dec⁻¹) and RuP₂@NPC (66.88 mV dec⁻¹), demonstrating its rapid reaction kinetics for the HERs. Accordingly, the prepared MoP-RuP₂@NPC possessed superior electrocatalytic performance for the HERs that was comparable with other previous nanomaterials (Table S1). The double-layer capacitance (Figure 3d) was related to the electrochemical surface areas (ECSA) of the designed electrocatalysts, which were investigated using capacitance measurements via cyclic voltammograms with different scan rates (Figure S5). The MoP-RuP₂@NPC exhibited a Cdl value of 3.61 mF cm⁻², which was higher than MoP@NPC (0.274 mF cm⁻²) and RuP₂@NPC catalysts (0.114 mF cm⁻²), as well as MP (0.157 mF cm⁻²). The high Cdl value of MoP-RuP₂@NPC implied the existence of abundant catalytic active sites, which led to its remarkable HER performance. Besides the catalytic activity, long-term durability is also an important factor for catalysts in practical applications. As illustrated in Figure 3e, the overpotential increased and remained high during the reversed process, indicating the excellent stability and mass transport properties. Moreover, MoP-RuP₂@NPC presented excellent long-term durability at a current density of 10 mA cm⁻² over 12 h (Figure 3f). Furthermore, MoP-RuP₂@NPC showed a similar initial HER performance after 2000 cycles of a cyclic voltammetry test (Figure S6). These observations suggest that the MoP-RuP₂@NPC possessed excellent stability for the HERs.

As MoP-RuP₂@NPC displayed excellent electrocatalytic performance and stability for the HERs in alkaline solution, a water-splitting electrolyzer was constructed by using the designed electrocatalysts as the cathode and commercial NiFe foam as the anode to drive an overall water-splitting process. As displayed in Figure 4a, an ultralow potential of 1.6 V was required to deliver a current density of 10 mA cm⁻² and the produced gases could be clearly observed in the picture (inset) and video (Movie S1). The electrolyzer composed of MoP-RuP₂@NPC exhibited electrocatalytic performances that were comparable to preceding catalysts, such as Ni₃S₂ [53], CoFeZr oxides/NF [54], β-Mo₂C [55], CoP NA/CC [56], Co/NBC-900 [57] and CoB-derived catalysts [58] (Figure 4b). Encouraged by the excellent catalytic performance, the electrolyzer setup with the developed MoP-RuP₂@NPC as a cathode could be successfully driven by a Stirling engine, where a large number of bubbles were generated in the electrodes (Figure 4c and Movie S2). In order to further evaluate the

practical application prospects, more tests were carried out and excellent performance was demonstrated. The designed electrolyzer could be powered using wind energy, a single AAA battery and solar energy (Figure S7 and Movies S3–S5). Furthermore, the long-term durability at a current density of 10 mA cm^{-2} was confirmed by a negligible decay after 12 h of measurement, suggesting its excellent overall water-splitting stability (Figure 4d). Thus, the prepared electrocatalyst has potential in practical applications for hydrogen production. The excellent electrocatalytic performance could be attributed to the following reasons: the abundant interfaces were important for boosting the catalytic performance; the interconnected pores allowed for favorable mass transport, exposing rich active sites and improving the release of generated bubbles; the heteroatom-doped carbon also contributed to enhancing the catalytic activity.

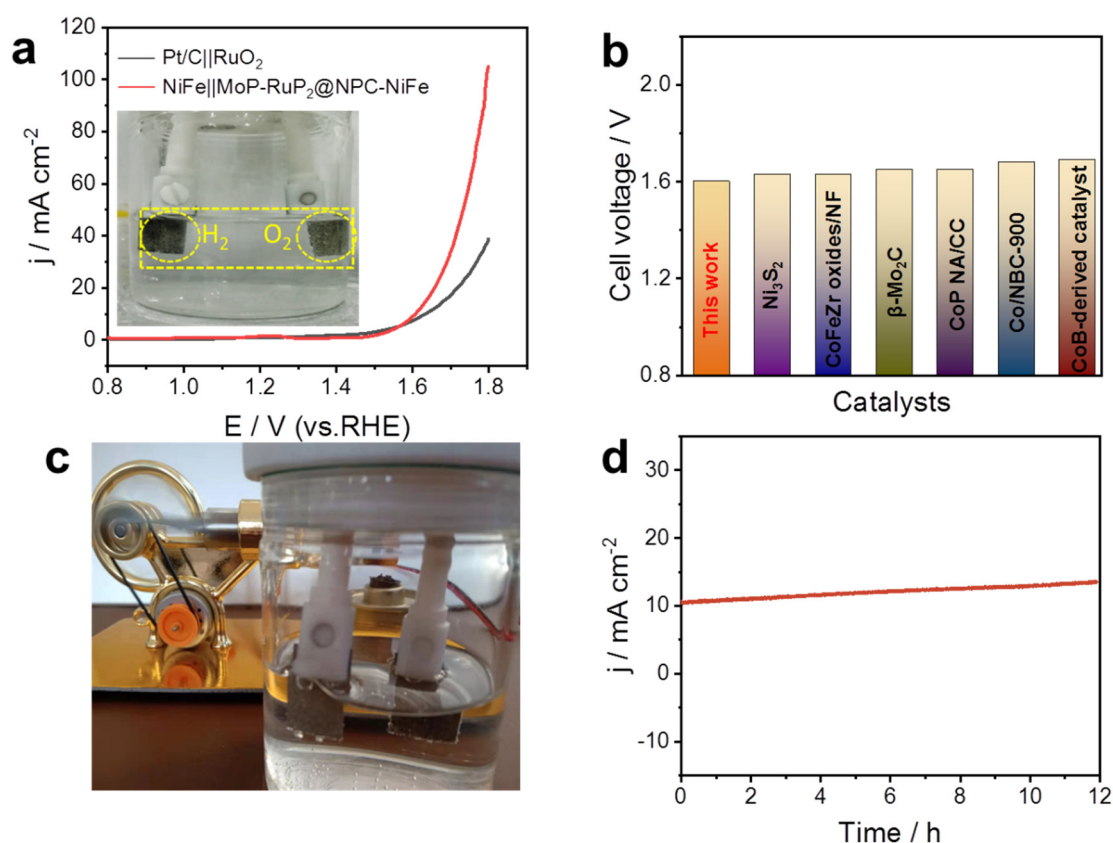


Figure 4. (a) Polarization curves of Pt/C||RuO₂ and NiFe||MoP-RuP₂@NPC-NiFe for overall water splitting in 1 M KOH. (b) Comparison of the overpotentials of the synthesized electrocatalysts with the reported values. (c) Electrochemical process powered using a Stirling engine. Chronoampermetry curve (d) of NiFe||MoP-RuP₂@NPC-NiFe.

4. Conclusions

In summary, MoP-RuP₂@NPC with abundant interfaces and rich pores was successfully prepared using a facile strategy with the low-toxic melamine phosphate as both the N and P source. The coupling effects and specific nanostructures endowed the designed nanomaterial with excellent electrocatalytic activity and long-term stability for the HERs. Moreover, MoP-RuP₂@NPC exhibited a superior overall water-splitting performance with a low overpotential of 1.6 V to drive 10 mA cm^{-2} . Moreover, sustainable energy sources, such as solar, thermal and wind, could be utilized to drive the electrolyzer, which could then store the intermittent energies as hydrogen energy. This work opens a convenient and sustainable strategy to develop efficient electrocatalysts for hydrogen production.

Supplementary Materials: The following are available online at <https://www.mdpi.com/article/10.3390/nano11092347/s1>, Figure S1. XRD patterns of RuP2@NPC (a) and MoP@NPC (b), Figure S2. Atomic concentrations of MoP-RuP2@NPC in XPS (at%), Figure S3. LSVs of MoP-RuP2@NPC with various different content for HER in 1 M KOH, Figure S4. LSVs of MoP-RuP2@NPC with different temperatures for HER in 1 M KOH, Figure S5. CV curves of MoP-RuP2@NPC (a), MoP@NPC (b), RuP2@NPC (c), MP (d) and Pt/C at different scan rate in 1M KOH, Figure S6. Stability test for MoP-RuP2@NPC via CV scanning for 2000 cycles in 1 M KOH for HER, Figure S7. The diagram of the electrocatalytic overall water-splitting with the electric energy generated by wind (a), solar (b), battery (c), Table S1. Comparison of the electrocatalytic performance toward HER in 1 M KOH, Movie S1. The movie of the electrocatalytic overall water-splitting, Movie S2. Electrocatalytic process powered using a Stirling engine, Movie S3. The movie of the electrocatalytic overall water-splitting with the electric energy generated by battery, Movie S4. The movie of the electrocatalytic overall water-splitting with the electric energy generated by wind wind, Movie S5. The movie of the electrocatalytic overall water-splitting with the electric energy generated by wind solar.

Author Contributions: Conceptualization, Z.W. and L.W.; methodology, Z.C. and Y.G.; writing—original draft preparation, Y.Z. and Z.C.; writing—review and editing, Z.W. All authors have read and agreed to the published version of the manuscript.

Funding: This work was financially supported by the the National Natural Science Foundation of China (22002068; 51772162, and 52072197); Youth Innovation and Technology Foundation of Shandong Higher Education Institutions, China (2019KJC004); Outstanding Youth Foundation of Shandong Province, China (ZR2019JQ14); Taishan Scholar Young Talent Program (tsqn201909114); Major Scientific and Technological Innovation Project (2019JZZY020405); and Major Basic Research Program of Natural Science Foundation of Shandong Province under grant no. ZR2020ZD09. This project was funded by the China Postdoctoral Science Foundation (2021M691700) and the Natural Science Foundation of Shandong Province of China (ZR2019BB002, ZR2018BB031).

Data Availability Statement: The data presented in this study are available on request from the corresponding author.

Conflicts of Interest: The authors declare no conflict of interest.

References

1. Liu, Y.; Feng, Q.; Liu, W.; Li, Q.; Wang, Y.; Liu, B.; Zheng, L.; Wang, W.; Huang, L.; Chen, L.; et al. Boosting interfacial charge transfer for alkaline hydrogen evolution via rational interior Se modification. *Nano Energy* **2021**, *81*, 105641. [[CrossRef](#)]
2. Hu, Q.; Wang, H.; Xiang, F.; Zheng, Q.; Ma, X.; Huo, Y.; Xie, F.; Xu, C.; Lin, D.; Hu, J. Critical roles of molybdate anions in enhancing capacitive and oxygen evolution behaviors of LDH@PANI nanohybrids. *Chin. J. Catal.* **2021**, *42*, 980–993. [[CrossRef](#)]
3. Liu, Q.; Wang, E.; Sun, G. Layered transition-metal hydroxides for alkaline hydrogen evolution reaction. *Chin. J. Catal.* **2020**, *41*, 574–591. [[CrossRef](#)]
4. Ren, H.; Sun, X.; Du, C.; Zhao, J.; Liu, D.; Fang, W.; Kumar, S.; Chua, R.; Meng, S.; Kidkhunthod, P.; et al. Amorphous Fe-Ni-P-B-O Nanocages as Efficient Electrocatalysts for Oxygen Evolution Reaction. *ACS Nano* **2019**, *13*, 12969–12979. [[CrossRef](#)] [[PubMed](#)]
5. Zhou, W.; Wu, M.; Li, G. Rambutan-like CoP@Mo-Co-O hollow microspheres for efficient hydrogen evolution reaction in alkaline solution. *Chin. J. Catal.* **2020**, *41*, 691–697. [[CrossRef](#)]
6. Song, M.; Zhang, Z.; Li, Q.; Jin, W.; Wu, Z.; Fu, G.; Liu, X. Ni-foam supported Co(OH)F and Co-P nanoarrays for energy-efficient hydrogen production via urea electrolysis. *J. Mater. Chem. A* **2019**, *7*, 3697–3703. [[CrossRef](#)]
7. Wen, Y.; Yang, T.; Cheng, C.; Zhao, X.; Liu, E.; Yang, J. Engineering Ru(IV) charge density in Ru@RuO2 core-shell electrocatalyst via tensile strain for efficient oxygen evolution in acidic media. *Chin. J. Catal.* **2020**, *41*, 1161–1167. [[CrossRef](#)]
8. Yang, J.; Chen, B.; Liu, X.; Liu, W.; Li, Z.; Dong, J.; Chen, W.; Yan, W.; Yao, T.; Duan, X.; et al. Efficient and Robust Hydrogen Evolution: Phosphorus Nitride Imide Nanotubes as Supports for Anchoring Single Ruthenium Sites. *J. Angew. Chem. Int. Ed.* **2018**, *5*, 9495–9500. [[CrossRef](#)]
9. Wu, Z.; Song, M.; Zhang, Z.; Wang, J.; Liu, X. Various strategies to tune the electrocatalytic performance of molybdenum phosphide supported on reduced graphene oxide for hydrogen evolution reaction. *J. Colloid Interface Sci.* **2019**, *536*, 638–645. [[CrossRef](#)] [[PubMed](#)]
10. Xie, H.; Lan, C.; Chen, B.; Wang, F.; Liu, T. Noble-metal-free catalyst with enhanced hydrogen evolution reaction activity based on granulated Co-doped Ni-Mo phosphide nanorod arrays. *Nano Res.* **2020**, *13*, 3321–3329. [[CrossRef](#)]
11. Cong, M.; Sun, D.; Zhang, L.; Ding, X. In situ assembly of metal-organic framework-derived N-doped carbon/Co/CoP catalysts on carbon paper for water splitting in alkaline electrolytes. *Chin. J. Catal.* **2020**, *41*, 242–248. [[CrossRef](#)]
12. Lao, J.; Li, D.; Jiang, C.; Luo, R.; Peng, H.; Qi, R.; Lin, H.; Huang, R.; Waterhouse, G.I.; Luo, C. Efficient overall water splitting using nickel boride-based electrocatalysts. *Int. J. Hydrog. Energy* **2020**, *45*, 28616–28625. [[CrossRef](#)]

13. Zhou, Y.-N.; Zhu, Y.-R.; Yan, X.-T.; Cao, Y.-N.; Li, J.; Dong, B.; Yang, M.; Li, Q.-Z.; Liu, C.-G.; Chai, Y.-M. Hierarchical CoSeS nanostructures assisted by Nb doping for enhanced hydrogen evolution reaction. *Chin. J. Catal.* **2021**, *42*, 431–438. [[CrossRef](#)]
14. Chen, L.; Song, Y.; Liu, Y.; Xu, L.; Qin, J.; Lei, Y.; Tang, Y. NiCoP nanoleaves array for electrocatalytic alkaline H₂ evolution and overall water splitting. *J. Energy Chem.* **2020**, *50*, 395–401. [[CrossRef](#)]
15. Geng, S.; Liu, Y.; Yu, Y.S.; Yang, W.; Li, H. Engineering defects and adjusting electronic structure on S doped MoO₂ nanosheets toward highly active hydrogen evolution reaction. *Nano Res.* **2019**, *13*, 121–126. [[CrossRef](#)]
16. Kim, J.; Jung, H.; Jung, S.M.; Hwang, J.; Kim, D.Y.; Lee, N.; Kim, K.S.; Kwon, H.; Kim, Y.T.; Han, J.W.; et al. Tailoring Binding Abilities by Incorporating Oxophilic Transition Metals on 3D Nanostructured Ni Arrays for Accelerated Alkaline Hydrogen Evolution Reaction. *J. Am. Chem. Soc.* **2021**, *143*, 1399–1408. [[CrossRef](#)] [[PubMed](#)]
17. Mathias, S.; David, T.; Lars, H.; Daniel, S.; Ulf-Peter, A. Fe/Co and Ni/Co-pentlandite type electro-catalysts for the hydrogen evolution reaction. *Chin. J. Catal.* **2021**, *42*, 1360–1369.
18. Wan, Z.; He, Q.; Chen, J.; Isimjan, T.T.; Wang, B.; Yang, X. Dissolution-regrowth of hierarchical Fe-Dy oxide modulates the electronic structure of nickel-organic frameworks as highly active and stable water splitting electrocatalysts. *Chin. J. Catal.* **2020**, *41*, 1745–1753. [[CrossRef](#)]
19. Zhao, J.; Ren, X.; Sun, X.; Zhang, Y.; Wei, Q.; Liu, X.; Wu, D. In situ evolution of surface Co₂CrO₄ to CoOOH/CrOOH by electrochemical method: Toward boosting electrocatalytic water oxidation. *Chin. J. Catal.* **2021**, *42*, 1096–1101. [[CrossRef](#)]
20. Zhang, L.; Liu, T.; Chen, N.; Jia, Y.; Cai, R.; Theis, W.; Yang, X.; Xia, Y.; Yang, D.; Yao, X. Scalable and controllable synthesis of atomic metal electrocatalysts assisted by an egg-box in algininate. *J. Mater. Chem. A* **2018**, *6*, 18417–18425. [[CrossRef](#)]
21. Wu, Z.; Zhao, Y.; Jin, W.; Jia, B.; Wang, J.; Ma, T. Recent Progress of Vacancy Engineering for Electrochemical Energy Conversion Related Applications. *Adv. Funct. Mater.* **2020**, *31*, 2009070. [[CrossRef](#)]
22. Li, Z.; Ge, R.; Su, J.; Chen, L. Recent Progress in Low Pt Content Electrocatalysts for Hydrogen Evolution Reaction. *Adv. Mater. Interfaces* **2020**, *7*, 2000396. [[CrossRef](#)]
23. Gu, M.; Jia, Q.; Zhu, Y.; Xu, L.; Tang, Y. In Situ Growth of Ultrafine Pt Nanoparticles onto Hierarchical Co₃O₄ Nanosheet-Assembled Microflowers for Efficient Electrocatalytic Hydrogen Evolution. *Chem. Eur. J.* **2020**, *26*, 15103–15108. [[CrossRef](#)]
24. Wang, J.; Zhang, Z.; Song, H.; Zhang, B.; Liu, J.; Shai, X.; Miao, L. Water Dissociation Kinetic-Oriented Design of Nickel Sulfides via Tailored Dual Sites for Efficient Alkaline Hydrogen Evolution. *Adv. Funct. Mater.* **2021**, *31*, 2008578. [[CrossRef](#)]
25. Lei, Y.; Wang, Y.; Liu, Y.; Song, C.; Li, Q.; Wang, D.; Li, Y. Designing Atomic Active Centers for Hydrogen Evolution Electrocatalysts. *Angew. Chem. Int. Ed.* **2020**, *59*, 20794–20812. [[CrossRef](#)] [[PubMed](#)]
26. Yan, Y.; Xia, B.; Li, N.; Xu, Z.; Fisher, A.; Wang, X. Vertically oriented MoS₂ and WS₂ nanosheets directly grown on carbon cloth as efficient and stable 3-dimensional hydrogen-evolving cathodes. *J. Mater. Chem. A* **2014**, *3*, 131–135. [[CrossRef](#)]
27. Lin, X.-Y.; Li, Y.-H.; Qi, M.-Y.; Tang, Z.-R.; Jiang, H.-L.; Xu, Y.-J. A unique coordination-driven route for the precise nanoassembly of metal sulfides on metal-organic frameworks. *Nanoscale Horiz.* **2020**, *5*, 714–719. [[CrossRef](#)] [[PubMed](#)]
28. Kagkoura, A.; Canton-Vitoria, R.; Vallan, L.; Hernandez-Ferrer, J.; Benito, A.; Maser, W.; Arenal, R.; Tagmatarchis, N. Bottom-Up Synthesized MoS₂ Interfacing Polymer Carbon Nanodots with Electrocatalytic Activity for Hydrogen Evolution. *Chem. Eur. J.* **2020**, *26*, 6635–6642. [[CrossRef](#)]
29. Xiong, Y.; Xu, L.; Jin, C.; Sun, Q. Interface-engineered atomically thin Ni₃S₂/MnO₂ heterogeneous nanoarrays for efficient overall water splitting in alkaline media. *Appl. Catal. B Environ.* **2019**, *254*, 329–338. [[CrossRef](#)]
30. Huang, X.; Xu, X.; Luan, X.; Cheng, D. CoP nanowires coupled with CoMoP nanosheets as a highly efficient cooperative catalyst for hydrogen evolution reaction. *Nano Energy* **2020**, *68*, 104332. [[CrossRef](#)]
31. Yu, J.; Wu, X.; Zhong, Y.; Yang, G.; Ni, M.; Zhou, W.; Shao, Z. Multifold Nanostructuring and Atomic-Scale Modulation of Cobalt Phosphide to Significantly Boost Hydrogen Production. *Chem.—Eur. J.* **2018**, *24*, 13800–13806. [[CrossRef](#)]
32. Yang, L.; Liu, R.; Jiao, L. Electronic Redistribution: Construction and Modulation of Interface Engineering on CoP for Enhancing Overall Water Splitting. *Adv. Funct. Mater.* **2020**, *30*, 1909618. [[CrossRef](#)]
33. Chen, J.; Ren, B.; Cui, H.; Wang, C. Constructing Pure Phase Tungsten-Based Bimetallic Carbide Nanosheet as an Efficient Bifunctional Electrocatalyst for Overall Water Splitting. *Small* **2020**, *16*, e1907556. [[CrossRef](#)]
34. Zhou, X.; Li, J.; Cai, X.; Gao, Q.; Zhang, S.; Yang, S.; Wang, H.; Zhong, X.; Fang, Y. In situ photo-derived MnOOH collaborating with Mn₂Co₂C@C dual co-catalysts boost photocatalytic overall water splitting. *J. Mater. Chem. A* **2020**, *8*, 17120–17127. [[CrossRef](#)]
35. Fu, W.; Wang, Y.; Tian, W.; Zhang, H.; Li, J.; Wang, S.; Wang, Y. Non-Metal Single-Phosphorus-Atom Catalysis of Hydrogen Evolution. *Angew. Chem. Int. Ed. Engl.* **2020**, *59*, 23791–23799. [[CrossRef](#)] [[PubMed](#)]
36. Zhao, Y.; Ling, T.; Chen, S.; Jin, B.; Vasileff, A.; Jiao, Y.; Song, L.; Luo, J.; Qiao, S. Non-metal Single-Iodine-Atom Electrocatalysts for the Hydrogen Evolution Reaction. *Angew. Chem. Int. Ed. Engl.* **2019**, *58*, 12252–12257. [[CrossRef](#)]
37. Yan, Y.; Xia, B.; Xu, Z.; Wang, X. Recent Development of Molybdenum Sulfides as Advanced Electrocatalysts for Hydrogen Evolution Reaction. *ACS Catal.* **2014**, *4*, 1693–1705. [[CrossRef](#)]
38. Xu, Y.; Wu, R.; Zhang, J.; Shi, Y.; Zhang, B. Anion-exchange synthesis of nanoporous FeP nanosheets as electrocatalysts for hydrogen evolution reaction. *Chem. Commun.* **2013**, *49*, 6656–6658. [[CrossRef](#)]
39. Sun, H.; Li, J.; Liu, L.; Ai, Y.; Hu, Z.; Xie, L.; Bao, H.; Wu, J.; Tian, H.; Guo, R.; et al. Facile and Large-Scale Fabrication of Porous Carbon Sheet Supported Sub-3 40. nm PtNi Nanoparticles: A Bifunctional Material for HER and Hydrogenation. *Chem. Eur. J.* **2019**, *25*, 7191–7200.

40. Pu, Z.; Amiin, I.S.; Kou, Z.; Li, W.; Mu, S. RuP₂-Based Catalysts with Platinum-like Activity and Higher Durability for the Hydrogen Evolution Reaction at All pH Values. *Angew. Chem. Int. Ed.* **2017**, *56*, 11559–11564. [[CrossRef](#)]
41. Yang, G.; Jiao, Y.; Yan, H.; Xie, Y.; Wu, A.; Dong, X.; Guo, D.; Tian, C.; Fu, H. Interfacial Engineering of MoO₂-FeP Heterojunction for Highly Efficient Hydrogen Evolution Coupled with Biomass Electrooxidation. *Adv. Mater.* **2020**, *32*, e2000455. [[CrossRef](#)]
42. Huang, Z.-F.; Song, J.; Pan, L.; Wang, Z.; Zhang, X.; Zou, J.-J.; Mi, W.; Zhang, X.; Wang, L. Carbon nitride with simultaneous porous network and O-doping for efficient solar-energy-driven hydrogen evolution. *Nano Energy* **2015**, *12*, 646–656. [[CrossRef](#)]
43. Zhang, H.; Liu, G.; Shi, L.; Ye, J. Single-Atom Catalysts: Emerging Multifunctional Materials in Heterogeneous Catalysis. *Adv. Energy Mater.* **2018**, *8*, 1701343. [[CrossRef](#)]
44. Wu, A.; Gu, Y.; Xie, Y.; Tian, C.; Yan, H.; Wang, D.; Zhang, X.; Cai, Z.; Fu, H. Effective Electrocatalytic Hydrogen Evolution in Neutral Medium Based on 2D MoP/MoS₂ Heterostructure Nanosheets. *ACS Appl. Mater. Interfaces* **2019**, *11*, 25986–25995. [[CrossRef](#)]
45. Paunović, P.; Gogovska, D.S.; Popovski, O.; Stoyanova, A.; Slavcheva, E.; Lefterova, E.; Iliev, P.; Dimitrov, A.T.; Jordanov, S.H. Preparation and characterization of Co–Ru/TiO₂/MWCNTs electrocatalysts in PEM hydrogen electrolyzer. *Int. J. Hydrogen Energy* **2011**, *36*, 9405–9414. [[CrossRef](#)]
46. Guo, B.-Y.; Zhang, X.-Y.; Xie, J.-Y.; Shan, Y.-H.; Fan, R.-Y.; Yu, W.-L.; Li, M.-X.; Liu, D.-P.; Chai, Y.-M.; Dong, B. Ultrafine RuP₂ nanoparticles supported on nitrogen-doped carbon based on coordination effect for efficient hydrogen evolution. *Int. J. Hydrogen Energy* **2021**, *46*, 7964–7973. [[CrossRef](#)]
47. Wu, Z.; Wang, J.; Liu, R.; Xia, K.; Xuan, C.; Guo, J.; Lei, W.; Wang, D. Facile preparation of carbon sphere supported molybdenum compounds (P, C and S) as hydrogen evolution electrocatalysts in acid and alkaline electrolytes. *Nano Energy* **2017**, *32*, 511–519. [[CrossRef](#)]
48. Wu, Z.; Wang, J.; Zhu, J.; Guo, J.; Xiao, W.; Xuan, C.; Lei, W.; Wang, D. Highly efficient and stable MoP-RGO nano-particles as electrocatalysts for hydrogen evolution. *Electrochim. Acta* **2017**, *232*, 254–261. [[CrossRef](#)]
49. Guo, L.; Cao, L.; He, J.; Huang, J.; Li, J.; Kajiyoshi, K.; Chen, S. Layered-structure (NH₄)₂Mo₄O₁₃@N-doped porous carbon composite as a superior anode for lithium-ion batteries. *Chem. Commun.* **2020**, *56*, 7757–7760. [[CrossRef](#)]
50. Muduli, S.; Rotte, N.K.; Naresh, V.; Martha, S.K. Nitrogen phosphorous derived carbons from Peltophorum pterocarpum leaves as anodes for lead–carbon hybrid ultracapacitors. *J. Energy Storage* **2020**, *29*, 101330. [[CrossRef](#)]
51. Gokhale, R.; Chen, Y.; Serov, A.; Artyushkova, K.; Atanassov, P. Novel dual templating approach for preparation of highly active Fe-N-C electrocatalyst for oxygen reduction. *Electrochim. Acta* **2017**, *224*, 49–55. [[CrossRef](#)]
52. Nagamuthu, S.; Ryu, K.-S. MOF-derived microstructural interconnected network porous Mn₂O₃/C as negative electrode material for asymmetric supercapacitor device. *CrystEngComm* **2019**, *21*, 1442–1451. [[CrossRef](#)]
53. Zheng, X.; Han, X.; Zhang, Y.; Wang, J.; Zhong, C.; Deng, Y.; Hu, W. Controllable synthesis of nickel sulfide nanocatalysts and their phase-dependent performance for overall water splitting. *Nanoscale* **2019**, *11*, 5646–5654. [[CrossRef](#)]
54. Huang, L.; Chen, D.; Luo, G.; Lu, Y.; Chen, C.; Zou, Y.; Dong, C.; Li, Y.; Wang, S. Zirconium-Regulation-Induced Bifunctionality in 3D Cobalt-Iron Oxide Nanosheets for Overall Water Splitting. *Adv. Mater.* **2019**, *31*, e1901439. [[CrossRef](#)]
55. Xing, J.; Li, Y.; Guo, S.; Jin, T.; Li, H.; Wang, Y.; Jiao, L. Molybdenum carbide in-situ embedded into carbon nanosheets as efficient bifunctional electrocatalysts for overall water splitting. *Electrochim. Acta* **2019**, *298*, 305–312. [[CrossRef](#)]
56. Liu, T.; Xie, L.; Yang, J.; Kong, R.; Du, G.; Asiri, A.M.; Sun, X.; Chen, L. Self-Standing CoP Nanosheets Array: A Three-Dimensional Bifunctional Catalyst Electrode for Overall Water Splitting in both Neutral and Alkaline Media. *ChemElectroChem* **2017**, *4*, 1840–1845. [[CrossRef](#)]
57. Liu, M.-R.; Hong, Q.-L.; Li, Q.-H.; Du, Y.; Zhang, H.-X.; Chen, S.; Zhou, T.; Zhang, J. Cobalt Boron Imidazolate Framework Derived Cobalt Nanoparticles Encapsulated in B/N Codoped Nanocarbon as Efficient Bifunctional Electrocatalysts for Overall Water Splitting. *Adv. Funct. Mater.* **2018**, *28*, 1801131. [[CrossRef](#)]
58. Chen, Z.; Kang, Q.; Cao, G.; Xu, N.; Dai, H.; Wang, P. Study of cobalt boride-derived electrocatalysts for overall water splitting. *Int. J. Hydrogen Energy* **2018**, *43*, 6076–6087. [[CrossRef](#)]